THE JOURNAL OF BIOLOGICAL CHEMISTRY Vol. 278, No. 20, Issue of May 16, pp. 18588–18596, 2003
Printed in U.S.A.

Crystal Structure of *Mycobacterium tuberculosis* Diaminopimelate Decarboxylase, an Essential Enzyme in Bacterial Lysine Biosynthesis*

Received for publication, February 13, 2003, and in revised form, March 3, 2003
Published, JBC Papers in Press, March 10, 2003, DOI 10.1074/jbc.M301549200

Kuppan Gokulan‡, Bernhard Rupp‡§, Martin S. Pavelka, Jr.¶‖, William R. Jacobs Jr.¶, and James C. Sacchettini‡ ‡‡**

*From the ‡Department of Biochemistry and Biophysics, Texas A&M University, College Station, Texas 77843-2128, the §Biology and Biotechnology Research Program, L-448, Lawrence Livermore National Laboratory, Livermore, California 94551, and the ¶Department of Microbiology and Immunology and the **Howard Hughes Medical Institute, Albert Einstein College of Medicine, The Bronx, New York 10461*

The *Mycobacterium tuberculosis lysA* gene encodes the enzyme *meso*-diaminopimelate decarboxylase (DAPDC), a pyridoxal-5′-phosphate (PLP)-dependent enzyme. The enzyme catalyzes the final step in the lysine biosynthetic pathway converting *meso*-diaminopimelic acid (DAP) to L-lysine. The *lysA* gene of *M. tuberculosis* H37Rv has been established as essential for bacterial survival in immunocompromised mice, demonstrating that *de novo* biosynthesis of lysine is essential for *in vivo* viability. Drugs targeted against DAPDC could be efficient anti-tuberculosis drugs, and the three-dimensional structure of DAPDC from *M. tuberculosis* complexed with reaction product lysine and the ternary complex with PLP and lysine in the active site has been determined. The first structure of a DAPDC confirms its classification as a fold type III PLP-dependent enzyme. The structure shows a stable 2-fold dimer in head-to-tail arrangement of a triose-phosphate isomerase (TIM) barrel-like α/β domain and a C-terminal β sheet domain, similar to the ornithine decarboxylase (ODC) fold family. PLP is covalently bound via an internal aldimine, and residues from both domains and both subunits contribute to the binding pocket. Comparison of the structure with eukaryotic ODCs, in particular with a difluoromethyl ornithine (DMFO)-bound ODC from *Trypanosoma bruceii*, indicates that corresponding DAP-analogues might be potential inhibitors for mycobacterial DAPDCs.

The final step in the bacterial lysine biosynthetic pathway is carried-out by *meso*-DAP[1] decarboxylase (DAPDC), encoded by the *lysA* gene. DAPDC is a vitamin B_6-dependent enzyme that stereospecifically converts *meso*-DAP to L-lysine (Scheme 1). Like most enzyme-catalyzed decarboxylation reactions, the conversion of DAP to lysine is not reversible. The enzyme is of interest because of its importance in bacterial growth and survival. Lysine is required in protein biosynthesis and is essential for bacterial viability and development. The lysine precursor DAP itself is used as a structural cross-linking component of the peptidoglycan layer of Gram-negative, Gram-positive (except Gram-positive *cocci*), and mycobacterial cell walls (1). DAP cross-links provide stability to the cell wall and confer resistance to intracellular osmotic pressure (2). DAP can be synthesized by one or more of the following three different pathways: (i) the succinylase pathway, identified in all Gram-negative and Gram-positive bacteria, as well as *Myobacterium tuberculosis*; (ii) the dehydrogenase pathway, utilized by *Bacillus sphaericus, Corynebacterium glutamicum*, and *Brevibacterium* species (3); and (iii) the acetylase pathway, which is limited to certain *Bacillus* species (4). Higher plants also produce lysine using a succinylase pathway (5). The presence of multiple biosynthetic pathways, at least in some bacteria, is probably an indication of the importance of DAP and lysine to bacterial survival. As the substrate and the reaction are not found in mammals, inhibitors of the enzyme may ultimately become leads for therapeutic intervention in bacterial infections (6).

In *Escherichia coli*, the *lysA* gene is transcriptionally controlled by the LysR regulator protein; in the presence of lysine, transcription of the *lysA* gene is repressed (7). In contrast, *M. tuberculosis* does not apparently have a comparable LysR regulator, based on the lack of homologous sequences in the *M. tuberculosis* genomic sequence (8). In *M. tuberculosis*, *C. glutamicum*, and *Brevibacterium lactofermentum*, the *lysA* gene is not in an operon as the second gene in an open reading frame with *argS* (arginyl-tRNA synthetase) (9–12). In *C. glutamicum* the *lysA* gene is constitutively expressed (11), and in the related organism *B. lactofermentum* the *lysA* gene is only weakly suppressed by lysine (12). Based on the evolutionary relationship between these three species of bacteria, we (13) proposed that the expression of the *lysA* gene of *M. tuberculosis* is probably constitutive.

* This work was funded by National Institutes of Health Grant P50 GM62410 (Tuberculosis Structural Genomics) and the Robert A. Welch Foundation. Use of the Argonne National Laboratory Structural Biology Center beamlines at the Advanced Photon Source was supported by the United States Department of Energy Office of Energy Research under contract number W-31-109-ENG-38. Use of BioCARS Sector 14 was supported by the National Institutes of Health, National Center for Research Resources. The Lawrence Livermore National Laboratory is operated by University of California for the United States Department of Energy under contract W-7405-ENG-48. The costs of publication of this article were defrayed in part by the payment of page charges. This article must therefore be hereby marked "*advertisement*" in accordance with 18 U.S.C. Section 1734 solely to indicate this fact.

‖ Present address: Dept. of Microbiology and Immunology, University of Rochester Medical Center, Rochester, NY 14642. Supported by a Burroughs Wellcome Fund Career Award in the Biomedical Sciences.

‡‡ To whom correspondence should be addressed. Tel.:979-862-7636; Fax: 979-862-7638; E-mail:sacchett@tamu.edu.

[1] The abbreviations used are: DAP, *meso*-diaminopimelic acid; DAPDC, *meso*-diaminopimelic acid decarboxylase; PLP, pyridoxal 5′-phosphate; ODC ornithine decarboxylase; SCID, severe combined immunodeficient; PBST, phosphate-buffered saline with Tween 80; CFU, colony-forming unit; MES, 4-morpholineethanesulfonic acid; APS, Advanced Proton Source; r.m.s.d., root mean square deviation; AR, alanine racemase; DFMO, α-difluoromethylornithine.

We show in this study that the *lysA* gene is essential for *M. tuberculosis* survival in an immunodeficient SCID (severe combined immunodeficient) mouse model, and we have determined the crystal structure of DAPDC in complex with the coenzyme pyridoxal 5′-phosphate (PLP) and the decarboxylation product lysine as well as DAPDC complexed with only lysine (binary complex). DAPDC is structurally very similar to eukaryotic ornithine decarboxylases (ODCs) (14–16) and, with the exception of a rotation of the C-terminal domain, to *Bacillus stearothermophilus* alanine racemase (AR) (17). Although both DAPDC and ODCs carry-out similar decarboxylation reactions involving pyridoxal-5′-phosphate (PLP) as a cofactor, DAPDC is the only known amino acid decarboxylase that stereospecifically acts on a substrate carbon atom in D-configuration (Scheme 1).

EXPERIMENTAL PROCEDURES

Generation and in Vitro Characterization of the lysA Mutant of M. tuberculosis—The *lysA* mutant of *M. tuberculosis*, mc^{2}3026, was previously constructed by allelic exchange and has a deletion within the coding region of the *lysA* gene with an inserted γδ resolvase binding site

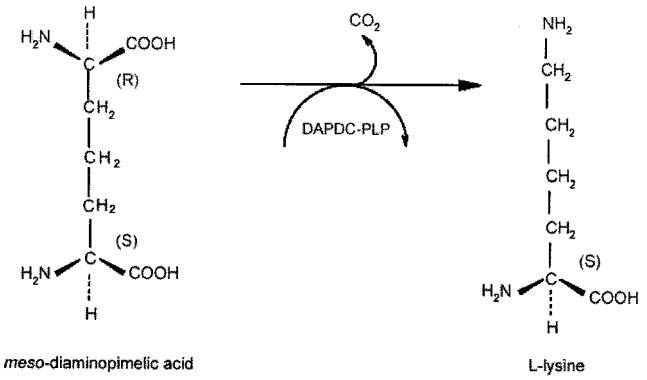

SCHEME 1. **Reaction schematic of stereospecific decarboxylation of *meso*-diaminopimelic acid (DAP) to L-lysine via vitamin B_6 (PLP)-dependent DAP-decarboxylase (DAPDC).**

(18). The mutant requires exogenous lysine supplementation at 1 mg/ml and can be complemented to protrophy by a copy of the wild-type *lysA* gene carried on the integrating vector pYUB651. In this work, we performed reversion analysis and were unable to isolate revertants from over 10^{10} *M. tuberculosis* Δ*lysA* cells. This established that the DAPDC activity can not be suppressed by any extragenic mutation and that the viability of the *M. tuberculosis* cells is dependent on this activity.

Clearance of the M. tuberculosis Lysine Auxotroph in SCID Mice—Female SCID mice were bred at the animal facility of the Albert Einstein College of Medicine. The animals were maintained under barrier conditions and fed sterilized commercial mouse chow and water *ad libitum*. The *M. tuberculosis* strains mc^{2}3026 (Δ*lysA5::res*) and mc^{2}3026 bearing pYUB651 (expressing the wild-type *lysA* gene) (13), were grown in Middlebrook 7H9 broth (Difco) supplemented with 0.05% Tween 80, 0.2% glycerol, and 1× ADS (0.5% bovine serum albumin, fraction V (Roche), 0.2% dextrose, and 0.85% NaCl) or on Middlebrook 7H10 or 7H11 solid medium (Difco) supplemented with 0.2% glycerol and 10% OADC (oleic acid, albumin, dextrose, and catalase; BD Biosciences). Cultures of the lysine auxotroph were supplemented with 1 mg/ml L-lysine (for both liquid and solid media), and 0.05% Tween 80 was added to solid medium. Liquid cultures were grown in 490-cm^2 roller bottles (Corning) at 4–6 rpm. Plates were incubated for 3–6 weeks.

Titered frozen stocks of bacteria were thawed and diluted appropriately in phosphate buffered saline containing 0.05% Tween 80 (PBST). The bacterial suspensions were plated at the time of injection to confirm viable counts. Intravenous injections were given via the tail vein. At various time points post-injection (24 h and once weekly), three mice were sacrificed for each strain, and the lungs, liver, and spleen were removed and homogenized separately in PBST using a Stomacher 80 (Tekmar, Cincinnati, OH). The homogenates were diluted in PBST and plated to determine the number of colony-forming units (CFU)/ml. Note that mice were sacrificed at 24 h post-injection in order to compare the bacterial colony-forming units received by the mice to the colony-forming units in the suspensions at the time of injection. Thus, the bacterial counts reported at time zero represent the viable bacteria present in the mice at 24 h post-injection.

Cloning of the lysA Gene and Expression of M. tuberculosis DAPDC—A 1.3-kb DNA fragment containing the *lysA* gene (Rv1237, Swiss Prot accession number P31848), was amplified by PCR with *M. tuberculosis* H37Rv genomic DNA as the template, using the following oligonucleotide primers: 5′-AGA GAA GCA TAT GAA CGA GCT

TABLE I
Anomalous data collection and phasing statistics for binary DAPDC-Lys complex

Data collection	Inflection (max f′)	Peak (max f″)	High remote
Wavelength (Å)	0.97917	0.97900	0.96380
Resolution range (Å)	81.4–2.9	81.4–2.9	65.7–2.9
Completeness (%)[a]	100 (100)	100 (100)	100 (100)
Completeness, 2σ (%)[a]	86 (67)	83 (56)	94 (85)
$\langle I/\sigma(I)\rangle$[a]	13.7 (2.8)	15.9 (2.6)	23.1 (7.2)
R(merge)[a] overall	0.069 (0.372)	0.063 (0.443)	0.039 (0.161)
f′ (e$^-$)	−10.26	−8.05	−3.06
f″ (e$^-$)	4.086	5.64	3.780
R(ano,λ)[a,b]			
Inflection	0.056 (0.127)	0.040 (0.098)	0.043 (0.101)
Peak		0.065 (0.146)	0.046 (0.130)
High			0.037 (0.083)

Phasing statistics								
Resolution bin (lower limit, Å)	9.9	6.3	5.0	4.2	3.7	3.4	3.2	2.9
F.o.m. initial (SOLVE)	0.79	0.71	0.62	0.52	0.38	0.29	0.19	0.14
F.o.m. final (SHARP, DM, NCS averaging)	0.92	0.87	0.88	0.82	0.73	0.62	0.59	0.41

[a] Values in parenthesis for the highest resolution bin (3.14–2.9 Å) for 2σ cutoff applied by SOLVE (100% without σ cutoff).
[b] Merging R(ano) for anomalous differences in diagonal elements and R(λ) for dispersive differences in off diagonal elements is shown below,

$$R_{(\mathrm{ano})} = \frac{\sum_{hkl}\|F^+| - |F^-\|}{\sum_{hkl}\frac{|F^+| + |F^-|}{2}} \quad R_{(\lambda(i,j\neq i))} = \frac{\sum_{hkl}\|F_{\lambda(i)}| - |F_{\lambda(j)}\|}{\sum_{hkl}|F_{\lambda(j)}|} \quad \text{F.o.m.} = \langle\cos(\alpha - \alpha_{(best)})\rangle_{bin}$$

where F.o.m. is figure of merit.

TABLE II
Data collection, refinement, and geometry statistics for binary and ternary DAPDC complexes

Data collection	DAPDC-Lys	DAPDC-PLP-Lys
Space group	$P4_12_12$	$P4_12_12$
Wavelength (Å)	0.96380	0.97918
Temperature (Kelvin)	120	120
a,b (Å)	111.6	111.5
c (Å)	237.7	238.2
Resolution (Å)	25.0–2.8	18.0–2.6
Highest resolution bin (Å)	2.87–2.8	2.67–2.6
Observed reflections[a]	813664 (58014)	276375 (19682)
Unique reflections[a]	35928 (2637)	44373 (3160)
% Completeness	99.9 (99.8)	99.8 (94.0)
R(merge)[a]	0.028 (0.136)	0.081 (0.405)
$\langle I/\sigma(I)\rangle$[a]	28.2 (7.5)	14.6 (3.1)
Vm (Matthews coefficient)	3.9	3.9
% Solvent	68	68
Refinement	**DAPDC-Lys**	**DAPDC-PLP-Lys**
Free R value, random, 5%[a]	0.247 (0.353)	0.268 (0.380)
R value[a]	0.192 (0.364)	0.224 (0.392)
Protein residues	892	890
Water molecules	204	230
Sulfate molecules	2	0
Lysine ligands	2	2
PLP ligands	0	2
R.m.s.d. bond length (Å)[b]	0.030	0.030
R.m.s.d. bond angle (Å)[b]	1.699	1.657
R.m.s.d. between subunits (Å)	0.331	0.410
Overall coordinate error (Å)[c]	0.309	0.281
RSCC (Shake&wARP)[d]	0.915	0.918
RSCC (Refmac5)[e]	0.939	0.941
Residue phi-psi angles	**DAPD-Lys**	**DAPD-PLP-Lys**
Most favored (%)	664 (87.3)	676 (88.7)
Allowed (%)	91 (12.0)	82 (10.7)
Generously allowed (%)	5 (0.7)	2 (0.3)
Disallowed (%)	0	2 (0.3)

[a] Values in parenthesis for the highest resolution bin.
[b] Deviations from restraint targets (44).
[c] Estimated standard uncertainty, diffraction precision index (DPI) based on free R (45).
[d] Real space correlation coefficient, averaged and weighted Shake&wARP map against F_c map.
[e] Real space correlation coefficient, maximum likelihood mF_o - DF_c map, reported by *Refmac5* (29). Additional details about chemical restraints and refinement parameters are available in the Protein Data Bank files 1HKW, 1HKV.

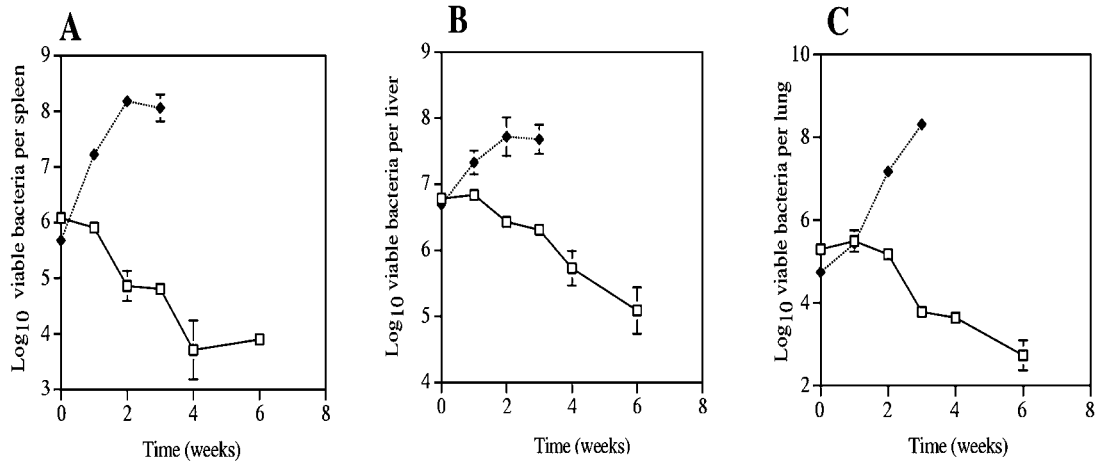

FIG. 1. **Clearance of the lysine auxotrophs in SCID mice.** The viable bacterial counts in CFU/ml are shown for the spleens, livers, and lungs of SCID mice injected intravenously with the various mycobacterial strains. Three mice were assayed at each time point. The *error bars* indicate the means ± S.D. Note that the counts at time zero are the counts obtained at 24 h post-injection as described under "Results and Discussion." *Panels A*, *B*, and *C* show the CFU/ml in each organ after injection with 1×10^7 CFU of the Lys$^-$ *M. tuberculosis* mutant mc^{2}3026 (*open squares*), or 1×10^7 CFU of the complemented Lys$^+$ *M. tuberculosis* strain mc^{2}3026/pYUB651 (*closed squares*).

GCT GCA CTT AGC GCC GAA TG-3′ and 5′-AGA GAA GGC GGC CGC CCT CAC TTC CAA ACT CAG CAA ATC GTC-3′. The amplified DNA fragment was digested with *Nde*I and *Not*I restriction enzymes and subcloned into the corresponding restriction sites in the pET30b vector with a C-terminal His_6 tag. *E. coli* B834 (DE3) Met$^-$ cells were transformed with the lysA-pET30b/His vector. The transformed cells were grown to exponential phase at 37 °C in TB media containing kanamycin. For production of Se-Met labeled protein, the cells were grown in M9 minimal media supplemented with all 19 standard amino acids and selenium-methionine (19). Expression of *lysA* was induced with 1 mM isopropyl-1-thio-β-D-galactopyranoside (IPTG), and cells were harvested after growth for 4–6 h at 16 °C.

DAPDC Purification—The harvested cells were pelleted and resuspended in buffer A (20 mM Tris-HCl, pH 8.0, and 50 mM imidazole)

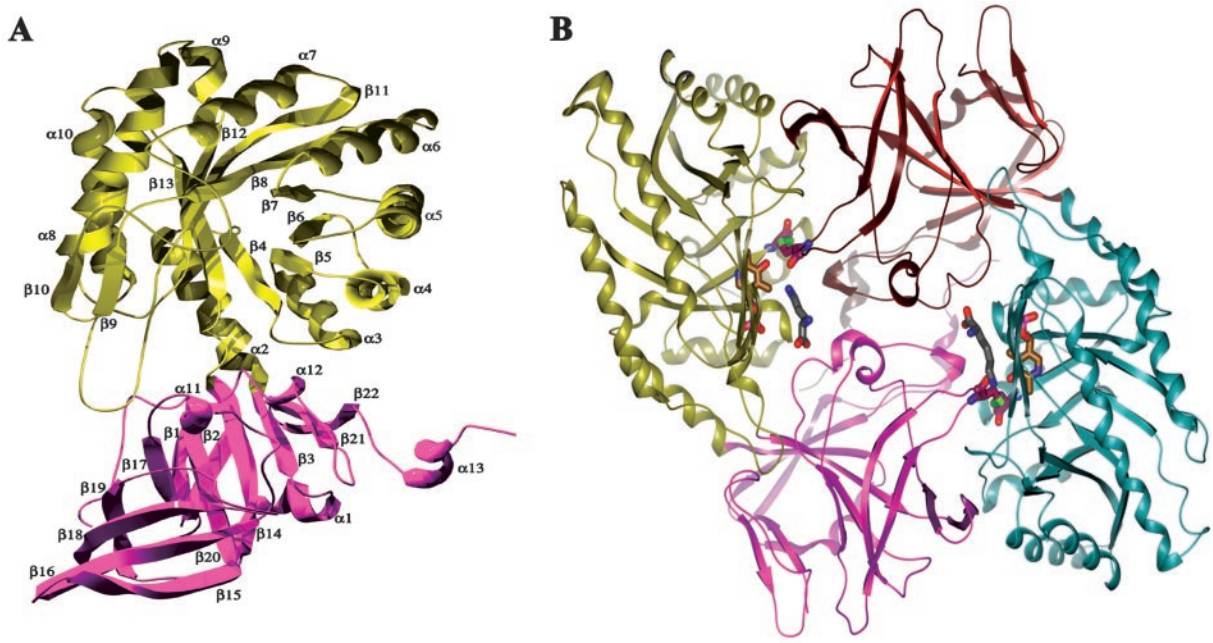

FIG. 2. **Overview of the *M. tuberculosis* DAPDC structure.** *A*, ribbon presentation of secondary structure elements. The α/β barrel domain (I) formed of residues 48–308 is shown in *yellow*; the C-terminal domain (II) contains residues 1–47 of the amino-terminal and 309–446 from the C-terminal region and is colored *magenta*. The fold is similar to that of eukaryotic ODCs and classifies *M. tuberculosis* DAPDC as a fold type III B_6-dependent enzyme. *B*, two molecules of DAPDC, related by 2-fold non-crystallographic symmetry, form a stable dimer. Subunit one, same color scheme as in *panel A*. Subunit two is colored *cyan* (N-terminal α/β domain) and *red* (C-terminal domain). Shown in *stick* representation, PLP and lysine, located in the binding pocket formed by dimer interfaces between N-terminal and C-terminal domains. Also shown are the disulfide links between the subunits.

containing 1 mM phenylmethylsulfonyl fluoride (PMSF) and complete EDTA-free protease inhibitors (Roche Applied Science). The cell mixture was repeatedly sonicated at 4 °C with 30 s pulses, and the cell suspension was centrifuged at 15,000 × *g* for 1 h. The clear supernatant was loaded onto an Amersham Biosciences Hi-trap Ni^{2+} chelating column and washed with 300 ml of buffer A containing 500 mM NaCl. The His-tagged DAPDC was eluted from the nickel affinity column using Buffer B (20 mM Tris-HCl, pH8.0, 500 mM imidazole, and 500 mM NaCl). After purification to near homogeneity by size exclusion chromatography (Amersham Biosciences) on an S-Superdex-200 column, DAPDC was dialyzed against 20 mM Tris buffer (pH 8.0), concentrated to 10 mg/ml, and stored in 20 mM Tris-HCl, pH 8.0, at −80 °C.

Crystallization—Native and Se-Met-labeled DAPDC (10 mg ml^{-1}) were crystallized at 18 °C by vapor diffusion in hanging drops. Initial crystallization screening was carried out with DAPDC alone, DAPDC incubated with DAP (5 mM) plus PLP (0.2 mM) overnight at 4 °C, and DAPDC plus lysine. Crystallization of DAPDC was only successful in the case of DAPDC supplemented with 5 mM lysine. Crystals (0.2 × 0.3 × 0.3 mm) grew at 18 °C within 3–7 days in 4-μl hanging drops (2 μl of DAPDC, 10 mg/ml, containing 5 mM of lysine combined with 2 μl of well solution) equilibrated against 500 μl of well solution containing 24% polyethylene glycol mono-methylether 5000 (PEG-MME 5000), 0.1 M MES buffer, pH 6.3, and 60 mM ammonium sulfate. Native DAPDC-lysine crystals were soaked for 3 h in mother liquor containing 0.2 mM PLP to obtain distinctly yellow-colored crystals of the DAPDC-PLP-lysine complex.

Data Collection—Highly redundant and complete selenium K-edge MAD diffraction data from a single Se-Met-DAPDC/lysine crystal were collected at three wavelengths using an ADSC CCD detector on beamline 14-ID-B at the Advanced Photon Source (APS) of the Argonne National Laboratory (ANL). Crystals mounted in cryo-loops were flash cooled in a N_2 stream (120 K) after brief soaks in 2 μl of mother liquor plus 2 μl of a cryoprotectant composed of 30% dioxane and 20% 2-methyl-2,4-pentanediol (MPD). Native data from DAPDC-PLP-lysine crystals were recorded on APS beamline 19BM using the 3 × 3 segment APS-1 CCD detector. The diffraction data were reduced using DENZO (20), and intensities were scaled with SCALEPACK (20). The reflections were indexed primitive tetragonal (a = b = 111.5 Å, c = 237.7 Å) with Laue symmetry 4/mmm. Examination of the integrated and scaled data indicated tetragonal space group $P4_12_12$ or its enantiomorph $P4_32_12$. Solvent content calculations (21) indicated the presence of either a dimer (V_M, 4.0; V_S, 70%) or a trimer (V_M, 2.8; V_S, 54%) in the asymmetric unit.

Structure Determination—Experimental phases for DAPDC-lysine were obtained by multiwavelength anomalous diffraction (MAD) phasing (22) (Table I). SHELXD located eight selenium sites in the asymmetric unit consistent with a dimer in the asymmetric unit (23), and SOLVE (24) was used to refine the sites and calculate initial protein phases, resulting in an overall figure of merit of 0.41 for the data in the resolution range of 100–2.8 Å. Further phase improvement with solvent flattening in AUTOSHARP (25) resulted in density-modified maps of high quality showing clear electron density for two molecules of protein in the asymmetric unit. The electron density map was submitted to TEXTAL (26) for automated model building. The TEXTAL model fit 80% of the backbone and 20% of the side chains correctly, with the exception of a stretch of 50 amino acids that were traced in the wrong direction; the remaining backbone model fit well into the electron density of the map. After determining the non-crystallographic symmetry (NCS) operator from the selenium substructure using graphical analysis and refinement with (CCP4) LSQKAB, the electron density was averaged and solvent flattened using DM (27). Starting from the TEXAL tracing, all of the residues of DAPDC except Met-1 could be built into the density-modified and -averaged experimental map using XTALVIEW (28). A final model of high quality was produced after several cycles of manual model building, and NCS restrained maximum likelihood refinement with REFMAC5 (29) against the high remote data set (Table II). A sulfate ion, located at the position of the PLP phosphate moiety, was clearly visible in the electron density. 204 water molecules were manually added during iterative cycles of model building and refinement. Weak electron density for the complexed lysine was visible in each binding pocket of the dimer but was not refined in the Se-Met model.

The structure of native DAPDC complexed with PLP and lysine was solved by molecular replacement with EPMR (30) (correlation coefficient 0.60) using the final model of the Se-Met DAPDC-lysine complex as a search model. Bias-minimized electron density maps were obtained using the Shake&wARP (SNW) protocol (31). Clear electron density for both PLP molecules and density for both lysines were visible in the Shake&wARP map prior to any model building. Several cycles of manual model adjustment and NCS-restrained maximum likelihood refinement in REFMAC5 yielded a final 2.6 Å model of good quality (Table II) for the DAPDC-PLP-lysine complex.

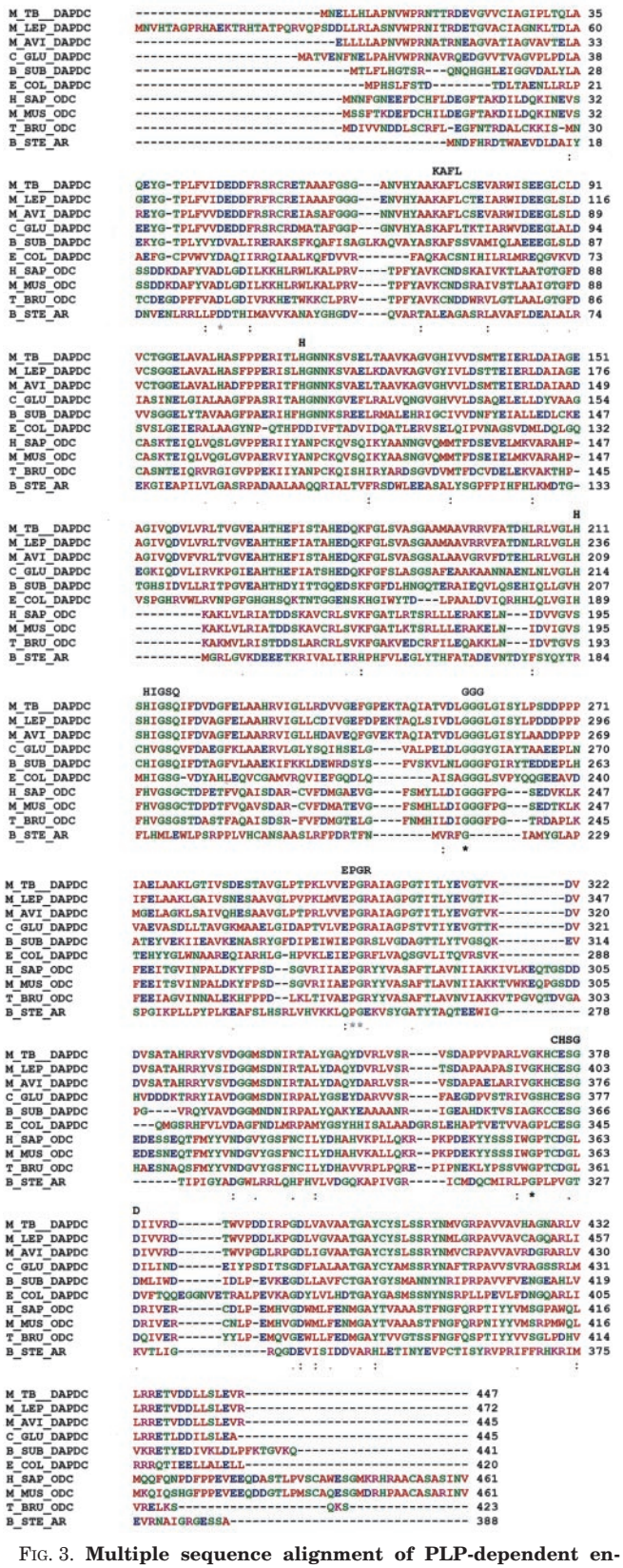

FIG. 3. **Multiple sequence alignment of PLP-dependent enzymes.** *Top line* indicates regions of partially conserved or important binding motives or residues. Alignment carried out with ClustalW 1.8.2 (40). Color key: *green*, polar residues; *red*, hydrophobic residues; *blue*, negatively charged; and *magenta*, positively charged.

RESULTS AND DISCUSSION

The lysA Gene Is Required for in Vivo Growth of M. tuberculosis H37Rv—The lysine auxotrophic strain mc^{2}3026 or the complemented mutant were each introduced (10^6 cells per mouse) into 24 SCID mice by tail vein injections, and groups of three mice each were sacrificed at 1 day post-injection and weekly thereafter until week 6. At each sacrifice, the number of viable bacteria was determined in the spleens, livers, and lungs of the mice. The lysine auxotrophic mutant was cleared from or did not grow in the examined organs of the SCID mice, whereas the complemented strain, mc^{2}3026/pYUB651, multiplied extensively (Fig. 1). In both the spleen and the lung, the number of viable bacteria decreased by three orders of magnitude in 6 weeks (Fig. 1*B*), whereas the decrease of the number of viable bacteria in the lung was only one order of magnitude (Fig. 1*C*). The mice given the complemented *M. tuberculosis* mutant died within 3 weeks, whereas the mice receiving the auxotrophic *M. tuberculosis* mutant did not display any gross organ pathology and survived for the duration of the experiment. Control experiments have demonstrated that immunocompetent C57BL/6 mice can clear an infection with the *M. tuberculosis* lysine auxotroph with the same kinetics as those seen for the clearance of the mutant in the spleen and lungs of the SCID mice (data not shown).

In addition, we tested the frequency of reversion of the *lysA* mutations by growing the mutant in the presence of lysine to mid-log phase of growth, centrifuging it, and resuspending it in media without lysine. The plating of two independent cultures and plating over 10^{10} cells from both cultures yielded no viable colonies, thus establishing that the lysA deletion mutant does not revert and cannot be suppressed by an extragenic mutation. The combination of the *in vitro* and *in vivo* data establishes that DAPDC activity is essential for the viability of *M. tuberculosis* and that *M. tuberculosis* cannot sequester lysine from a mammalian host. We thus reasoned that drugs targeted against DAPDC could be effective anti-tuberculosis agents and pursued the determination of the three-dimensional structure of *M. tuberculosis* DAPDC.

Overview of the M. tuberculosis DAPDC Structure—The crystal structure of M. tuberculosis DAPDC confirms its classification as a fold type III B_6 dependent enzyme (32). DAPDC has a fold similar to eukaryotic ODCs (14–16), and DAPDC also forms a stable head-to-tail homodimer of practically identical subunits with a coordinate deviation comparable with the overall r.m.s.d. coordinate error for the structure models (0.33 and 0.42 Å, respectively).

Each of the DAPDC subunits (related by proper 2-fold rotation) consists of two ODC-like domains (Fig. 2). Domain I is composed of residues 48–308 forming a α/β barrel comprised of β-strands (β4–β13) and helices (α2–α10). The first 47 residues are located in domain II and contain strands β1, β2, β3, and helix α1, leading into helix α2 of the barrel. The C-terminal domain II contains residues 2–47 (β1, β2, β3, and α1) and 309–446 (α11–α13, strands β14–β21) and forms a mixed β-sheet flanked by α helices. The two structural domains are connected by helix α2 and β13. All of the loops connecting the β strands and α helices were clearly visible in the electron density.

Two identical binding sites are formed by residues of both polypeptide chains of the dimer. The active site is at the interface between the α/β barrel domain of one subunit and the β sheet domain of both subunits. Residues from the α/β barrel are mainly involved in binding PLP, whereas residues from the β sheet domain primarily contribute to substrate binding. Large conformational changes between the binary DAPDC-lysine and ternary DAPDC-PLP-lysine complex are absent (overall Cα coordinate r.m.s.d. 0.42 Å). The only significant differences between the DAPDC complex structures appear near the substrate and cofactor binding sites, discussed below.

TABLE III
Sequence and structure alignment summary for fold type III PLP dependent enzymes

SwissProt Accession Number (TIGR contig for *M. avium*)	Organism and function	Interdimer S-S bond	PDB code	Reference to structure	Sequence alignment identity to *M.tb.*	R.m.s.d. to *M. tuberculosis* monomer	Buried dimer surface(Å^2).
						Å	*Å^2, %*
P31848	*M. tuberculosis DAPDC*	YES	1HKV				3462, 21.0
Q50140	*M. leprae*[a] *DAPDC*	YES			86		
3294	*M. avium*[b] *DAPDC*	YES			85		
P09890	*C. glutamicum DAPDC*				57		
P23630	*B. subtilis*[c] *DAPDC*				41		
P00861	*E. coli DAPDC*				27		
P11926	*H. sapiens*[d] *ODC*		1D7K	(16)	17	2.27	2516, 13.5
P00860	*M. musculus*[e] *ODC*		7ODC	(15)	16	2.22	2239, 13.4
P07805	*T. bruceii ODC*		2TOD	(34)	18	2.16	2021, 13.2
P10724	*B. stearothermophilus AR*		1SFT	(17)	5	2.70	2944, 19.6

[a] *Myobacterium leprae.*
[b] *Myobacterium avium.*
[c] *Bacillus subtilis.*
[d] *Homo sapiens.*
[e] *Mus musculus.*

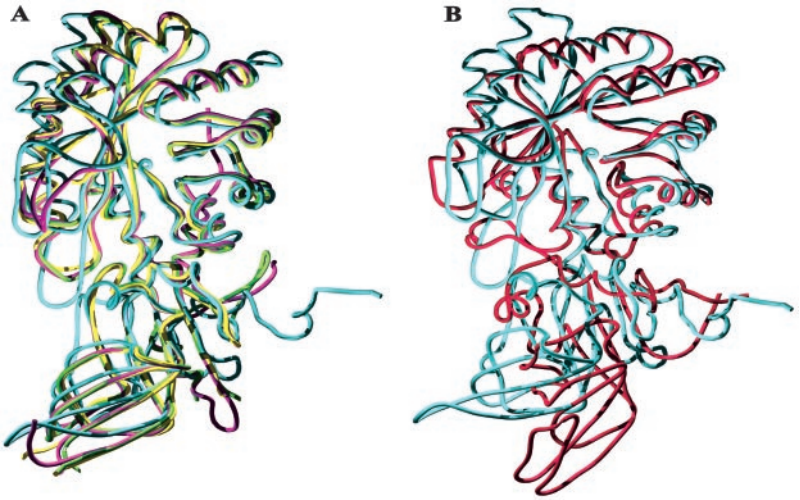

FIG. 4. **Backbone superposition of known fold type III PLP-dependent enzyme structures.** *Panel A*, color key: *cyan*, *M. tuberculosis* DAPDC; *magenta*, human ODC; *green*, mouse ODC; and *yellow*, *T. brucei*. *Panel B*, superposition of *M. tuberculosis* DAPDC (*cyan*) with *B. stearothermopilus* AR (*red*). The rotation of the AR β-domain relative to the other structures is clearly visible. The superpositions were carried by the Local-Global-Alignment server (Adam Zemla, predictioncenter.llnl.gov/local/lga/lga.html); corresponding r.m.s.d. values are listed in Table III. The figure was prepared using Swiss Pdb Viewer (41) and PovRay (www.povray.org).

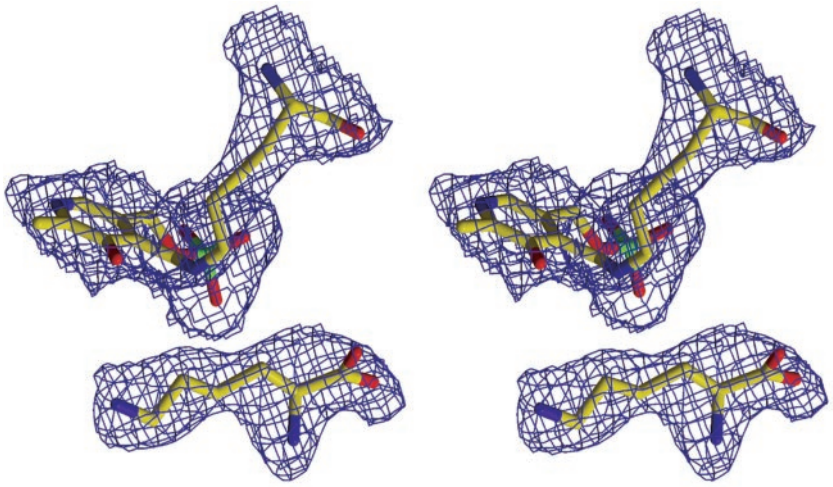

FIG. 5. **Electron density in the DAPDC binding cleft for covalently bound PLP and lysine.** Both PLP and lysine were omitted from the model before map generation (Shake&wARP map (31) contoured at 1 σ level). The blob feature in XtalView has been used to limit the display of the electron density within 2 Å of the model. This figure was created by XtalView (28) and rendered with Raster3d (42).

Comparison of M. tuberculosis DAPDC with Eucaryotic Ornithine Decarboxylases and Alanine Racemase—A search for structural alignment using DALI (33) revealed high similarity (Z-value 34.4) with eukaryotic ODCs, enzymes found in the polyamine biosynthetic pathway catalyzing the decarboxylation of ornithine to putrescine and a lower level of structural similarity with AR from *B. stearothermophilus* (Z-value, 18.3). Multiple sequence alignments of known mycobacterial DAPDC sequences, eukaryotic ODCs with known structures, and *B. stearothermopilus* AR are presented in Fig. 3 and summarized together with structural data in Table III. Despite the relatively low level of amino acid sequence identity between eukaryotic ODCs and *M. tuberculosis* DAPDC (~18%), least squares superposition of the structures indicates close resem-

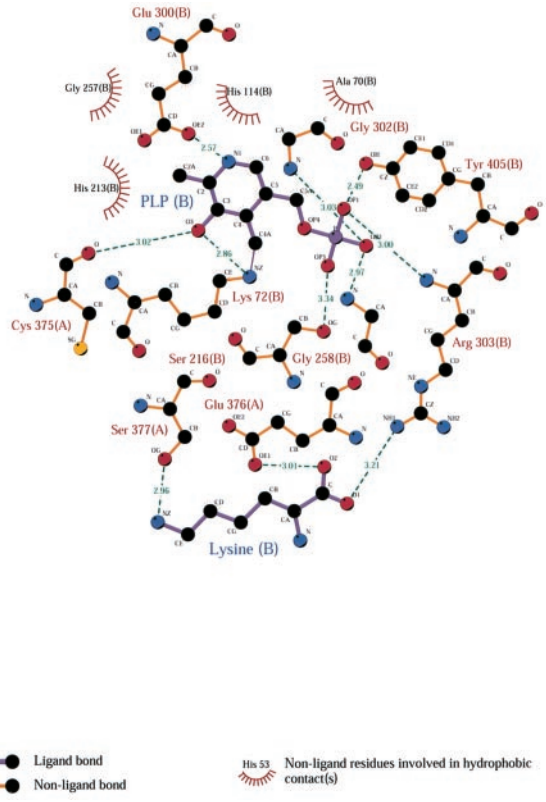

FIG. 6. **Schematic representation of ligand binding interactions in active site pocket of DAPDC.** Residues of both homodimer subunits contribute to PLP and to lysine binding. This figure was created by LIGPLOT (43).

blance (r.m.s.d. values, ~2.2 Å). Even AR, which shares only 5% identity with DAPDC, superimposes with 2.7 Å r.m.s.d. (Fig. 4). The higher deviation can be attributed largely to a distinct rotation of the AR β-domain respective to the well superimposing α/β barrels (~30°, see also Grishin *et al.* 1999 (34)).

The sequence alignments (Fig. 3) also show a decreasing conservation of PLP binding motives from the mycobacterial DAPDCs to the eukaryotic ODCs and AR. The KAFL motif, containing the lysine residue that covalently binds to PLP via Schiff base (internal aldimine) formation, is conserved in procaryotic DAPDCs and eukaryotic ODCs, as is the glycine rich motif (GGG) shown to interact with the phosphate group of PLP. Other conserved motifs include the HIGS motif (thought to be involved in protonation/deprotonation reactions), and the EPGR and CESGD motifs, which are part of the substrate binding regions (35). These motifs, however, with the exception of EPGR, appear not conserved in the structurally related alanine racemase, consistent with its very low sequence identity to the DAPDCs.

Comparison of the large, buried, solvent-accessible surface area at the dimer interface (Table III) indicates that DAPDC (3462 $Å^2$, or 21%) forms the most stable dimer among the fold type III members of known structure. The extensive number of conserved intermolecular contacts and the absence of extended crystal packing contacts (largest contact area between symmetry related subunits in the crystal lattice is 64 $Å^2$) indicate that DAPDC is an obligate dimer. Additional structural support for the dimer as the functional unit comes from the unexpected finding of a disulfide bridge between Cys-93 of one subunit of the dimer and Cys-375 of the other subunit. Intersubunit disulfide bridges are very rare in cytoplasmic proteins, especially in prokaryotes. Cys-93 is found only in mycobacterial DAPDCs but is absent in all other bacterial DAPDCs. Cys-375 also forms a hydrogen bond via its backbone oxygen to the PLP OP3 hydroxyl group of the other subunit and is conserved in all bacterial DAPDCs as well as in other type III B_6-dependent enzymes. Chromatographic experiments further provide chemical evidence that *M. tuberculosis* DAPDC is indeed a stable dimer. DAPDC migrated with an apparent molecular weight consistent with a dimer in gel filtration chromatography experiments, and the disulfide bridge adjoining the two subunits was confirmed by non-reducing SDS-PAGE (not shown). Interestingly, early ultracentrifugation studies reported that *E. coli* DAPDC was a tetramer (36), whereas gel filtration analysis suggested that the *E. coli* DAPDC enzyme was monomeric (37). For *M. tuberculosis* DAPDC, neither the crystal structure nor size exclusion chromatography nor the native SDS gels described above support a monomeric state or the formation of a tetramer.

The PLP-binding Site—The active site of *M. tuberculosis* DAPDC is located in a shallow, highly hydrophilic cavity between the dimer interfaces with the deep PLP binding pocket located near the C-terminal ends of the β strands of the α/β barrel, similar to other ODCs (14–16). Clear electron density for PLP was visible in the SNW omit maps of the ternary complex and indicated the presence of a covalent C=N link between Lys-72 Nϵ and C4A of PLP (Fig. 5).

Hydrogen bonds and nonbonding contacts between PLP and DAPDC are summarized in Fig. 6. The oxygen atoms of the PLP phosphate group hydrogen bond with the peptide backbone nitrogen atoms of Gly-258 in the glycine rich motif and those of Gly-302 and Arg-303. OP1 also forms a hydrogen bond with the hydroxyl group of Tyr-405. In the DAPDC-lysine binary complex, a sulfate ion occupies the same position as the phosphate group of PLP in the ternary DAPDC-PLP-lysine structure.

In addition to the covalent link to Lys-72 Nϵ, the pyridyl moiety of PLP is positioned by a hydrogen bond to the side-chain carboxylate of Glu-300, which participates in an extended hydrogen bond network with Asp-91 and the conserved residues Asp-254 and His-211. Two histidine residues (114 and 213) and Ala-70 form hydrophobic contacts, with His-213 π-stacking against the *si* face of the pyridine ring. His-114 and Asp-91 are positioned toward the *re* face of the pyridine ring, and both are within hydrogen bonding distance of the carboxylate of Glu-300. The network of interactions around Glu-300 in the binding pocket essentially fixes the position of the imidazole side chains of His-114 and His-211, as well as the carboxylates of Asp-91 and Asp-254 with respect to the pyridine ring of PLP. An additional hydrogen bond to the other subunit of the dimer exists between the O3 hydroxyl group of PLP(B) and the backbone oxygen of the disulfide forming cysteine Cys-375A (Fig. 6).

The side chain of His-213 π-stacks with the *si* side of the pyridyl ring. This residue is conserved in the eukaryotic ODCs; however, His-211 and His-114 are absent and are replaced by serine and alanine or glycine, respectively. In *B. stearothermopilus* AR, the π-stacked His-213 is again conserved via AR His-166, and His-211 and His-114 are replaced by Tyr-164 and Leu-85. The highly variable environment on the *re* face of the pyridyl ring caused by these residue substitutions could play a significant role in fine-tuning the (stereo)specificity and/or pH optimum of the different PLP-mediated reactions in these enzymes.

Lysine Binding to M. tuberculosis DAPDC—In the DAPDC-PLP-lysine complex, the density for reaction product lysine could be located in each binding site. In binding site B, the density is very clear and allowed unambiguous positioning and

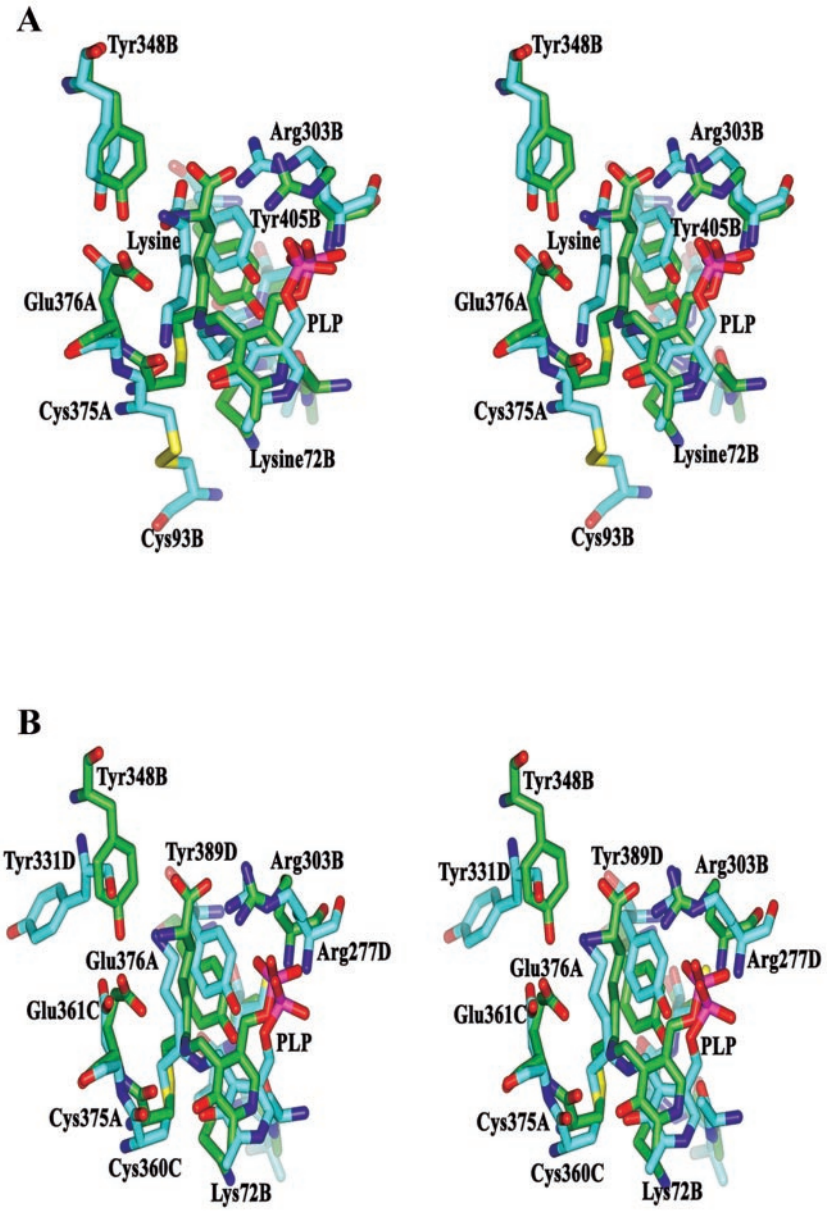

FIG. 7. **Stereoviews of superpositions of the active sites of the two models.** *A*, superposition of energy-minimized models of putative DAPDC-inhibitor (DFDAP) complex (*green* carbon backbone) with ternary DAPDC-PLP-Lysine complex (*cyan* carbon backbone) are shown in stereo. The aminocarboxyl group on the PLP-bound DFDAP molecule occupies a position similar to lysine in the ternary DAPDC complex. The DAPDC-DFDAP was modeled covalently bound to Cys-375A, causing speculation that breakage of the Cys-375A to Cys-93B intersubunit disulfide bond could occur through an attack of a highly reactive fluorinated imine intermediate (35). *B*, superposition of the putative DAPDC-inhibitor (DFDAP) complex (*green* carbon backbone) with the *T. bruceii* ODC-DFMO complex (*cyan* carbon backbone), showing the similarity in the overall geometry of the bound inhibitors in stereo. *T. bruceii* ODC-DFMO was superimposed onto the structure of DAPDC to achieve a crude positioning of the PLP-DFMO complex in the active site of the tuberculosis (TB) enzyme. The PLP-DFMO complex was extended to the corresponding bound PLP-DFDAP analog, and the starting position was adjusted. Hydrogens were added, and the docked model was refined further with BioMedCaChe (v.6.0a1). Valence and hybridization checks were enabled and improved hydrogen bond lengths and van der Waals interactions. The structure of DAPDC with the bound PLP-DFDAP analog complex was optimized using the Bio-MM2 molecular mechanics engine in CaChe.

refinement of the lysine molecule (Fig. 5). In site A, the lysine is again oriented similarly to the first site, but its exact position along the channel opening in the binding site is not as clear as for site B. Both lysines are positioned with the side chain toward the *si* face of the PLP pyridyl ring, consistent with decarboxylation occurring on this side of the ring. Residues of domain II of the other subunit (Ser-377A, Glu 376A) participate in lysine binding consistent with the important role of ODC Asp-361 (corresponding to DAPDC Glu-376) that has been demonstrated in Ala mutation studies (38), which show a 2000-fold decrease in substrate binding affinity in mODC. The carboxyl group of lysine is further fixed by conserved residue Arg-303, which participates in PLP binding via backbone N contacts as well. As clearly visible in the electron density Fig. 5, the ϵ-amino group and CE of lysine are positioned reasonably close (~4.0 Å) to the catalytic Schiff base formed by the Lys-PLP internal aldimine. (Fig. 5). A model of the substrate DAP based on the bound lysine would thus have its (D)-aminoacyl group in a position to interact with the internal aldimine from the *si* side of the pyridoxyl ring as well as with conserved His-213, Arg-161, and possibly Ser-377.

Given the limited 2.6 Å resolution of the present structure, further discussion of the details of the stereospecificity of the decarboxylation mechanism in DAPDC must remain speculative. The structural similarity between the DAPDC binding site and that of eukaryotic ODCs suggests a related mechanism. The catalytic mechanism of the decarboxylation reaction preformed by ODCs has been extensively studied (14, 38). The major difference is that in ODCs the amino acid substrate ornithine is in an L configuration, but DAPDC decarboxylates the D-aminocarboxyl group of *meso*-DAP. Details in the orientation of the D-aminocarboxyl group with respect to the conjugated pyridyl ring system acting as an electron sink as well as stereospecificity of the anchoring of the non-reacting L-aminocarboxyl group through the domain II residues are likely responsible for achieving stereospecific decarboxylation of DAP. Amino acid decarboxylation reactions of fold type III PLP-dependent enzymes generally occur on the *si* side of the pyridyl ring plane (as discussed by Kern *et al.* in 1999 (15)), and evidence exists that the reaction may involve an inversion of the reactive Cα of the substrate (39).

Structural Basis of DAPDC as a Potential Anti-tuberculosis Drug Target—The comparison of DAPDC with the inhibitor- and product-bound ODC structures (14, 32) of the parasitic

flagellate *Trypanosoma brucei* indicates that DAPDC, given that it is essential for *M. tuberculosis* viability, could be a potential anti-mycobacterial drug target. Although there are currently no known drugs that target DAPDC, one of the most widely used drugs used to treat African sleeping sickness is α-difluoromethylornithine (DFMO), a suicide inhibitor that targets *T. brucei* ODC (32). In the crystal structure, DFMO forms the external aldimine linkage with PLP as seen in the product-bound structure (14), but in addition it is covalently bound to the side chain of Cys-360, thus irreversibly blocking the binding site (Fig. 5). A slight backbone torsion, combined with an ~160° rotation of the equivalent Cys-375 SG, suffices to bring DAPDC into practically the same conformation as the DFMO-bound *T. brucei* ODC (Fig. 7) but necessitates the breakage of the intersubunit disulfide bond in DAPDC. It has been proposed that in ODCs DFMO decarboxylation via the internal PLP aldimine followed by elimination of a F^- anion might form a highly reactive electrophilic imine, attacking the nucleophilic Cys-360 thiol group (35). To what degree a reactive imine of a fluorinated DAP analogue might be capable of attacking the Cys-375-Cys-93 disulfide bond, is unknown. It certainly would require a transient conformational rearrangement, probably associated with a slight rotation of PLP, which now has lost its covalent link, to position the reactive imine so that a reaction can take place. Provided the disulfide bond gets broken, the product conformation would closely resemble the arrangement found in DFMO-bound ODC. An energy-minimized model, starting from a DAP molecule placed just as the bound DFMO in the *T. brucei* x-ray structure, shows that the same conformation is conceivable for a putative DAPDC-inhibitor complex, with quite satisfying geometry (Fig. 7). Stereospecificity of the decarboxylation reaction preceding the attack of the reactive imine intermediate would likely require that a DAP analog be stereospecifically fluorinated at the D-aminocarboxyl group of DAP.

Acknowledgments—We acknowledge Katherine Kantardjieff, Center for Molecular Structure, California State University, Fullerton, for ligand docking and minimization calculations on the putative DAPDC-inhibitor complex. B. R. thanks James C. Sacchettini, Texas A&M University, and the Lawrence Livermore National Laboratory for support of his sabbatical leave at Texas A&M University. We thank Ms. Linda Fisher for preparation of the manuscript and Ms. Stephanie Swanson for technical assistance.

REFERENCES

1. Cummins, C. S., and Harris, H. (1996) *J. Gen. Microbiol.* **14,** 583–600
2. Strominger, J. L. (1962) *Fed. Proc.* **21,** 134–143
3. Misono, H., Nagasaki, S., and Soda, K. (1986) *Agric. Biol. Chem.* **50,** 1455–1460
4. Sundharadas, G., and Gilvarg, C. (1967) *J. Biol. Chem.* **242,** 3983–3984
5. Chatterjee, S. P., Singh, B. K., and Gilvarg, C. (1994) *Plant Mol. Biol.* **26,** 285–290
6. McCann, P. P., and Pegg, A. E. (1992) *Pharmacol. Ther.* **54,** 195–215
7. Stagier, P., Brone, F., Richard, F., Richard, C., and Patte, J. C. (1983) *J. Bacteriol.* **156,** 1198–1203
8. Cole, S. T., Brosch, R., Parkhill, J., Garnier, T., Churcher, C., Harris, D., Gordon, S. V., Eiglmeier, K., Gas, S., Barry, C. E., III, Tekaia, F., Badcock, K., Basham, D., Brown, D., Chillingworth, T., Connor, R., Davies, R., Devlin, K., Feltwell, T., Gentles, S., Hamlin, N., Holroyd, S., Hornsby, T., Jagels, K., Krogh, A., McLean, J., Moule, S., Murphy, L., Oliver, K., Osborne, J., Quail, M. A., Rajandream, M.-A., Rogers, J., Rutter, S., Seeger, K., Skelton, J., Squares, R., Squares, S., Sulston, J. E., Taylor, K., Whitehead, S., and Barrell, B. G. (1998) *Nature* **393,** 537–544
9. Andersen, A. B., and Hansen, E. B. (1993) *Gene* **124,** 105–109
10. Sharp, P. M., and Mitchell, K. J. (1993) *Mol. Microbiol.* **8,** 200
11. Marcel, T., Archer, J. A., Mengin-Lecreulx, D., and Sinskey, A. J. (1990) *Mol. Microbiol.* **4,** 1819–1830
12. Oguiza, J. A., Malumbres, M., Eriani, G., Pisabarro, A., Mateos, L. M., Martin, F., and Martin, J. F. (1993) *J. Bacteriol.* **175,** 7356–7362
13. Pavelka, M. S., Jr., and Jacobs, W. R., Jr. (1996) *J. Bacteriol.* **178,** 6496–6507
14. Jackson, L. K., Brooks, H. B., Osterman, A. L., Goldsmith, E. J., and Phillips, M. A. (2000) *Biochemistry* **39,** 11247–11257
15. Kern, A. D., Oliveira, M. A., Coffino, P., and Hackert, M. L. (1999) *Structure Fold. Des.* **7,** 567–581
16. Almrud, J. J., Oliveira, M. A., Kern, A. D., Grishin, N. V., Phillips, M. A., and Hackert, M. L. (2000) *J. Mol. Biol.* **295,** 7–16
17. Shaw, J. P., Petsko, G. A., and Ringe, D. (1997) *Biochemistry* **36,** 1329–1342
18. Pavelka, M. S., Jr., and Jacobs, W. R., Jr. (1999) *J. Bacteriol.* **181,** 4780–4789
19. Miller, J. H. (1972) *Experiments in Molecular Genetics*, pp. 431–435, Cold Spring Harbor Laboratory, Cold Spring Harbor, NY
20. Otwinowski, Z., and Minor, W. (1997) *Methods Enzymol.* **276,** 307–326
21. Matthews, B. W. (1968) *J. Mol. Biol.* **33,** 491–497
22. Hendickson, W. A., and Ogata, C. M. (1997) *Methods Enzymol.* **276,** 494–523
23. Sheldrick, G. M., and Gould, R. O. (1995) *Acta Crystallogr. Sect. B Struct. Crystallogr. Cryst. Chem.* **51,** 423–431
24. Terwilliger, T. C., and Berendzen, J. (1999) *Acta Crystallogr. Sect. D Biol. Crystallogr.* **55,** 849–861
25. Cowtan, K. D., and Main, P. (1996) *Acta Crystallogr. Sect. D Biol. Crystallogr.* **52,** 43–48
26. Ioerger, T. R., Holton, T., Christopher, J. A., and Sacchettini, J. C. (1999) *Proc. Int. Conf. Intell. Syst. Mol. Biol.* 130–137
27. Cowtan, K. D., and Zhang, K. Y. J. (1999) *Prog. Biophys. Mol. Biol.* **72,** 245–270
28. McRee, D. E. (1999) *J. Struct. Biol.* **125,** 156–165
29. Murshudov, G. N., Vagin, A. A., and Dodson, E. J. (1997) *Acta Crystallogr. Sect. D Biol. Crystallogr.* **53,** 240–255
30. Kissinger, C. R., Gehlharr, D. K., and Fogel, D. B. (1999) *Acta Crystallogr. Sect. D Biol. Crystallogr.* **55,** 484–491
31. Kantardjieff, K. A., Höchtl, P., Segelke, B. W., Tao, F.-M., and Rupp, B. (2002) *Acta Crystallogr. Sect. D Biol. Crystallogr.* **58,** 735–743
32. Grishin, N. V., Phillips, M. A., and Goldsmith, E. J. (1995) *Protein Sci.* **4,** 1291–1304
33. Holm, L., and Sander, C. (1995) *Trends Biochem. Sci.* **20,** 478–480
34. Grishin, N. V., Osterman, A. L., Brooks, H. B., Phillips, M. A., and Goldsmith, E. J. (1999) *Biochemistry* **38,** 15174–15184
35. Poulin, R., Lu, L., Ackermann, B., Bey, P., and Pegg, A. E. (1992) *J. Biol. Chem.* **267,** 150–158
36. White, P., and Kelley, B. (1965) *Biochem. J.* **96,** 75–84
37. Bourot, S., Sire, O., Trautwetter, A., Touze, T., Wu, L. F., Blanco, C., and Bernard, T. (2000) *J. Biol. Chem.* **275,** 1050–1056
38. Osterman, A. L., Kinch, L. N., Grishin, N. V., and Phillips, M. A. (1995) *J. Biol. Chem.* **270,** 11797–11802
39. Asada, Y., Tanizawa, K., Nakamura, K., Moriguchi, M., and Soda, K. (1984) *J. Biochem. (Tokyo)* **95,** 277–282
40. Thompson, J. D., Higgins, D. G., and Gibson, T. J. (1994) *Nucleic Acids Res.* **22,** 4673–4680
41. Guex, N., and Peitsch, M. C. (1997) *Electrophoresis* **18,** 2714–2723
42. Merritt, E. A., and Murphy, M. E. P. (1994) *Acta Crystallogr. Sect. D Biol. Crystallogr.* **50,** 869–873
43. Wallace, A. C., Laskowski, R. A., and Thornton, J. M. (1995) *Protein Eng.* **8,** 127–134
44. Engh, R., and Huber, R. (1991) *Acta Crystallogr. Sect. A* **47,** 392–400
45. Cruickshank, D. W. J. (1999) *Acta Crystallogr. Sect. D Biol. Crystallogr.* **55,** 583–601